

Influence of Intermediate Principal Stress on the Strength and Dilatancy Behavior of Rockfill Material

Yang Xiao, S.M.ASCE¹; Hanlong Liu²; Yumin Chen³; and Jian Chu⁴

Abstract: The mechanical behaviors of rockfill materials at a comparatively low pressure are very important (e.g., for the stability of the top part and the slope of rockfill dams). In addition, the stress conditions of rockfill dams are unlikely to be axisymmetric but are three-dimensional. Because of this, the influence of the intermediate principal stress has to be taken into consideration in design. This paper presents a study on the effect of intermediate principal stress on the strength and dilatancy behavior of rockfill material at a comparatively low pressure. A series of constant b -value tests were carried out on rockfill materials commonly used for earth dam construction. Using the test data, the influences of the b -value on the peak friction angle, critical-state friction angle, and maximum dilatancy angle of rockfill materials were investigated. A revised relative dilatancy index was proposed for rockfill material to describe the change in the shear strength with the intermediate principal stress. The relationship among the incremental friction angle, the maximum dilatancy angle, and the b -value was examined. A linear relationship between the incremental friction angle and the revised relative dilatancy index was established by considering the effect of the b -value. The predictions given by this relationship agree well with experimental data. Furthermore, the b -value can influence the particle breakage of rockfill materials, indicating that such breakage is dependent on the stress path. DOI: 10.1061/(ASCE)GT.1943-5606.0001178. © 2014 American Society of Civil Engineers.

Author keywords: Rockfill material (RFM); Intermediate principal stress; Peak friction angle; Critical-state friction angle; Dilatancy angle; Relative dilatancy index.

Introduction

The relationships between the peak friction angle and the maximum dilatancy angle of sands have been studied by many researchers (Bolton 1986; Vaid and Sasitharan 1992; Salgado et al. 2000; Yang and Li 2004; Lashkari 2009; Chakraborty and Salgado 2010). Common agreement among these studies is as follows (Bolton 1986): (1) the secant value of the friction angle is the basis for discussion; (2) understanding the dilatancy toward critical states is central to an understanding of soil behavior; and (3) both stress and density affect the rate of dilatancy of soils and therefore their strength parameters. A new relative dilatancy index was proposed by Bolton (1986) to capture variations in the peak friction angle of sands, and it was widely used in penetration resistance theory (Salgado et al. 1997a, b, 1998; Salgado and Randolph 2001). The new relative dilatancy index has the advantage of ensuring that zero dilatancy is achieved at the

critical effective stress (Bolton 1986). The relative dilatancy index pertaining to the peak friction angle was validated by triaxial and plane-strain tests of sands. However, the relationship between the peak friction angle and the maximum dilatancy angle has not been fully investigated in general stress paths. It is uncertain whether this relationship is dependent on the Lode angle or the b -value.

Rockfill material (RFM) is the main material used in the construction of rockfill dams and railways. The mechanical behavior of this material has not been investigated as intensively as that of sands. The strength and deformation behaviors of RFMs have been mainly investigated by large-scale triaxial apparatuses (Marsal 1967; Leps 1970; Marschi et al. 1972; Charles and Watts 1980; Varadarajan et al. 1997; Indraratna et al. 1998; Varadarajan et al. 1999; Gupta 2000; Varadarajan et al. 2003; Kohgo et al. 2007; Lackenby et al. 2007; Anderson and Fair 2008; Gupta 2009a, b; Lashkari 2009; Daouadji and Hicher 2010; Seif El Dine et al. 2010; Sevi and Ge 2012; Vasistha et al. 2012; Xu et al. 2012; Fu et al. 2013; Vasistha et al. 2013; Zhang et al. 2013; Xiao et al. 2014a, b), as well as through oedometer apparatuses (Matheson 1986; Oldecop and Alonso 2011) and via the discrete-element method (Lobo-Guerrero et al. 2006; Zhou et al. 2013). In addition, a multiaxial testing device (Desai et al. 1982; Desai and Faruque 1984; Desai et al. 1995; Desai and Toth 1996) was used to investigate the strength and stress-strain behavior of gravel soils (Janardhanam and Desai 1983; Desai and Salami 1987; Desai and El-Hoseiny 2005). True triaxial tests on RFM (Shi 2008) were also carried out to investigate strength (Xiao et al. 2011b, 2012) and dilatancy (Xiao et al. 2011a) under different loading paths.

Charles and Watts (1980) emphasized that the mechanical behaviors of RFMs at comparatively low pressure were much more important in most field cases [e.g., the top part and the slope of high rockfill dams, low rockfill dams (smaller than 50 m), and embankments]. The typical confining pressure in such field cases would be unlikely to be greater than 400 kPa (Charles and Watts 1980).

¹Associate Professor, College of Civil Engineering, Chongqing Univ., Chongqing 400450, China; Researcher, College of Civil and Transportation Engineering, Hohai Univ., Nanjing 210098, China. E-mail: hhxyanson@163.com

²Professor and Chair, College of Civil Engineering, Chongqing Univ., Chongqing 400450, China. E-mail: cehliu@cqu.edu.cn

³Associate Professor, College of Civil and Transportation Engineering, Hohai Univ., Nanjing 210098, China (corresponding author). E-mail: ymchenhhu@163.com

⁴Professor, Dept. of Civil, Construction and Environmental Engineering, Iowa State Univ., Ames, IA 50011. E-mail: jchu@iastate.edu

Note. This manuscript was submitted on August 24, 2013; approved on July 15, 2014; published online on August 4, 2014. Discussion period open until January 4, 2015; separate discussions must be submitted for individual papers. This paper is part of the *Journal of Geotechnical and Environmental Engineering*, © ASCE, ISSN 1090-0241/04014064(15)/\$25.00.

Indraratna et al. (1993) also pointed out that the strength and deformation behaviors of RFMs at a lower confining pressure were significant in most real-life situations. Natural, coarse, granular soils [e.g., Scoria deposit (Agustian and Goto 2008) and colluvial soils (Zhao et al. 2013), which are widely distributed in the natural slopes] possess very low confining pressures. The RFMs [under the lower confining pressure from the slopes of the Lyn Brianne Dam and Scammonden Dam during and after construction, as investigated by Charles (1975)] are more likely to exhibit dilation behavior. This could be mainly because the lower confining pressure could not suppress the dilation of the RFMs. The question arises as to whether the stress state of the RFM in the slope of a rockfill dam approaches the failure state. A stress-dilatancy relation is required to answer this question (Charles 1975). Moreover, the stress conditions of the field cases (as mentioned previously) would be unlikely to be axisymmetric but are three-dimensional. Therefore, this paper aims mainly to investigate the three-dimensional stress-dilatancy of RFMs at a comparatively low confining pressure.

Scope

The main objective of this paper was to systemically investigate the peak friction angle, critical-state friction angle, and maximum dilatancy angle of RFM at different b -values and minor principal stresses through a series of true triaxial tests. A revised relative dilatancy index, based on the work of Bolton (1986), was proposed to capture the variation in the peak friction angle of RFM with the b -value. Furthermore, the relationship between the peak friction angle and the maximum dilatancy angle of the RFM was established by incorporating the b -value based on the true triaxial test results of the RFM.

Definitions of Strength and Stress and Strain Parameters

Stress Definitions

The deviatoric stress q and mean effective stress p' are defined as

$$p' = \frac{\sigma_1 + \sigma_2 + \sigma_3}{3} \quad (1a)$$

$$q = \frac{1}{\sqrt{2}} \sqrt{(\sigma_1 - \sigma_2)^2 + (\sigma_2 - \sigma_3)^2 + (\sigma_3 - \sigma_1)^2} \quad (1b)$$

where σ_1 , σ_2 , and σ_3 = major, intermediate, and minor effective stresses, respectively.

The stress ratio η is given as

$$\eta = \frac{q}{p'} \quad (2)$$

The b -value is defined as

$$b = \frac{\sigma_2 - \sigma_3}{\sigma_1 - \sigma_3} \quad (3)$$

The b -value in the following true triaxial tests is kept as a constant. Eq. (3) can be rewritten as

$$(\sigma_2 - \sigma_3) - b(\sigma_1 - \sigma_3) = 0 \quad (4)$$

The derivation of Eq. (4) (with the conditions $db = 0$ and $d\sigma_3 = 0$ because the b -value and the confining pressure σ_3 are

kept as constants in the following true triaxial tests for RFM) gives

$$\begin{aligned} (d\sigma_2 - d\sigma_3) - db(\sigma_1 - \sigma_3) - b(d\sigma_1 - d\sigma_3) &= 0 \\ db &= 0 \\ d\sigma_3 &= 0 \\ \Rightarrow d\sigma_2 &= bd\sigma_1 \\ \Rightarrow (d\sigma_2)_i &= b_i(d\sigma_1)_i \end{aligned} \quad (5)$$

The subscript i = loading step i . The value of $d\sigma_2$ at each loading step can be determined by Eq. (5) when the b -value and the major stress increment $d\sigma_1$ are specified during shearing. Based on Eq. (3), the b -value at the i step can be given as

$$(b)_i = \frac{(\sigma_2)_i - (\sigma_3)_i}{(\sigma_1)_i - (\sigma_3)_i} \quad (6)$$

The b -value at the $i + 1$ step [with the condition $(d\sigma_3)_i = 0$] can be given as

$$\begin{aligned} (b)_{i+1} &= \frac{(\sigma_2)_{i+1} - (\sigma_3)_{i+1}}{(\sigma_1)_{i+1} - (\sigma_3)_{i+1}} \\ &= \frac{[(\sigma_2)_i + (d\sigma_2)_i] - [(\sigma_3)_i + (d\sigma_3)_i]}{[(\sigma_1)_i + (d\sigma_1)_i] - [(\sigma_3)_i + (d\sigma_3)_i]} \\ &= \frac{[(\sigma_2)_i - (\sigma_3)_i] - (d\sigma_2)_i}{[(\sigma_1)_i - (\sigma_3)_i] - (d\sigma_1)_i} \end{aligned} \quad (7)$$

The combination of Eqs. (5)–(7) gives

$$\begin{aligned} (b)_{i+1} &= \frac{[(\sigma_2)_i - (\sigma_3)_i] - (d\sigma_2)_i}{[(\sigma_1)_i - (\sigma_3)_i] - (d\sigma_1)_i} \\ &= \frac{(b)_i [(\sigma_1)_i + (d\sigma_1)_i] - (b)_i (d\sigma_1)_i}{[(\sigma_1)_i + (d\sigma_1)_i] - (d\sigma_1)_i} = (b)_i \end{aligned} \quad (8)$$

Consequently, the b -value is kept as a constant during shearing.

Friction Angle Definitions

The mobilized friction angle ϕ_m is defined as

$$\sin \phi_m = \frac{\sigma_1 - \sigma_3}{\sigma_1 + \sigma_3} \quad (9)$$

The peak friction angle ϕ_p is defined as the maximum mobilized friction angle ϕ_m in the process of shearing, and the critical-state friction angle ϕ_{cs} is defined as the mobilized friction angle ϕ_m at the constant volumetric strain under the drained compression condition.

Dilatancy Definitions

The maximum dilatancy angle θ_{\max} (ignoring the elastic strain) is defined as follows (Yang and Li 2004):

$$\sin \theta_{\max} = \frac{2}{3} \left| \frac{d\varepsilon_v}{d\varepsilon_s} \right|_{\max} = \frac{2}{3} |d|_{\max} \quad (10)$$

where $d\varepsilon_v$ and $d\varepsilon_s$ = increments of the volumetric strain and shear strain, respectively; and d = dilatancy.

A well-known empirical relative dilatancy index proposed by Bolton (1986) was used to describe the peak friction angle of sands pertaining to the density and pressure

$$I_R = I_D [Q - \ln(p')] - R \quad (11)$$

where Q and R = state index constants of material; and p' = mean effective stress at the failure state. The relative density I_D can be expressed as

$$I_D = \frac{e_{\max} - e}{e_{\max} - e_{\min}} \quad (12)$$

where e = void ratio; e_{\min} = minimum void ratio; and e_{\max} = maximum void ratio.

Material for Testing

The RFM from the Yalong River in West China was used for testing. This alluvium material contains mainly granite and conglomerate, and its unconfined compressive strength (ASTM 2010) is approximately 113.5 MPa. The aggregate impact value and aggregate crushing value [European Committee for Standardization (CEN) 2010] of this material are 22.6 and 30.8%, respectively. The particle size of the RFM, as shown in Fig. 1(a), was reduced by the parallel gradation technique (Lowe 1964). The particle size density curve of the RFM is shown in Fig. 1(b). The particle shape of the RFM was rounded/subrounded, and the particle size was smaller than 10 mm. The uniformity coefficient C_u and the curvature coefficient C_c of the RFM were 19.2 and 2.5, respectively. The specimen was divided into five equal parts for compacting inside the split mold. The initial void ratio e_0 and the initial relative density I_D of the RFM were 0.26 and 0.85, respectively, which indicates that the RFM was in an initial dense state.

Testing Apparatus and Testing Procedure

Testing of the RFM was conducted by the true triaxial apparatus (TTA) (ASTM 2014). The vertical load in the loading system (as shown in Fig. 2) is applied through a rigid plate. One of the horizontal loads was applied to the specimen by a composite plate (i.e., a set of specially designed elastic blocks, as shown in Fig. 2), which was flexible in the vertical direction. The other horizontal load (i.e., the sum of the minor principal stresses) was applied by hydrostatic pressure. The TTA (Xiao et al. 2011a) has a digital operation system, a controlling system, and a loading system. The interaction between the plates and the water bag increases greatly when the confining pressure σ_3 is larger than 500 kPa. This restricts the application of the TTA when the confining pressure is high. The specimen size of the TTA is 120 mm in length, 60 mm in width, and 120 mm in height (as shown in Fig. 3). The testing procedure was as follows:

1. The specimen was compacted in the split mold with five equal parts, and the vacuum pump was used to stabilize the specimen;
2. The rigid plate, composite plate, and water pressure bag were assembled;
3. A confining pressure was first applied to the specimen; the minor principal stress σ_3 and the b -value were kept as constants during shearing; the values of the minor principal stress σ_3 and the b -value are listed in Table 1, and Fig. 4 shows the stress paths of the RFM at $\sigma_3 = 200$ kPa; and
4. The specimen was sheared under dry conditions with a constant major strain rate (i.e., 1 mm/min); the test ended when the major strain reached 15%.

The volume change is the sum of the displacements in the σ_1 , σ_2 , and σ_3 directions, which are measured by LVDTs on the platens. The

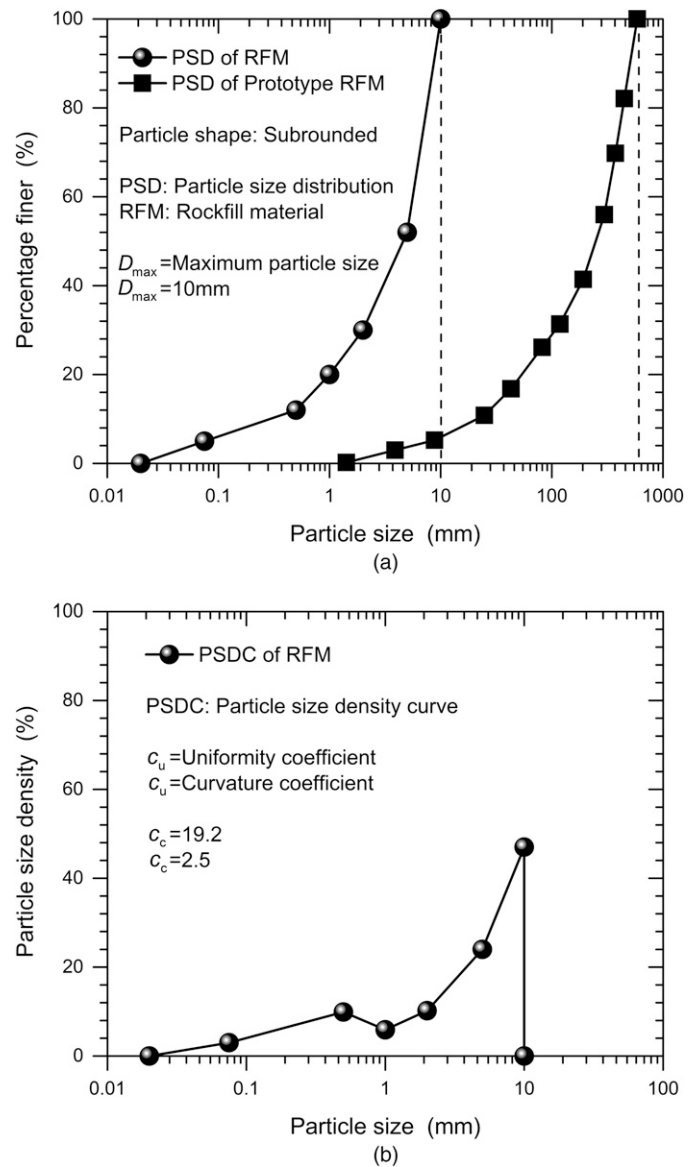


Fig. 1. RFM in true triaxial tests: (a) particle size distribution; (b) particle size density curve

number of true triaxial tests was 20 for the RFM. The specimen of RFM showed a bulging failure mode (with no obvious shearing band or nonhomogeneous deformation), which indicated that strain softening is a property of RFM (Chu et al. 1996).

Test Results

For a concrete-face rockfill dam, the RFM is mainly in a dry condition because of the impervious concrete face. For a clay-core rockfill dam, the upstream rockfill is in a drained condition, whereas the downstream rockfill is mainly in a dry condition. In this paper, three independent drained tests at $\sigma_3 = 100$ kPa were carried out to compare the stress-strain behaviors of RFM in drained and dry conditions. It can be seen from Fig. 5 that the RFM exhibits almost a similar stress-strain behavior, although the peak strength of the dry sample is slightly higher than that of the saturated sample. This could be attributed to the fact that the RFM possesses a rounded particle shape and a high particle strength. The water effect for this RFM could be ignored.

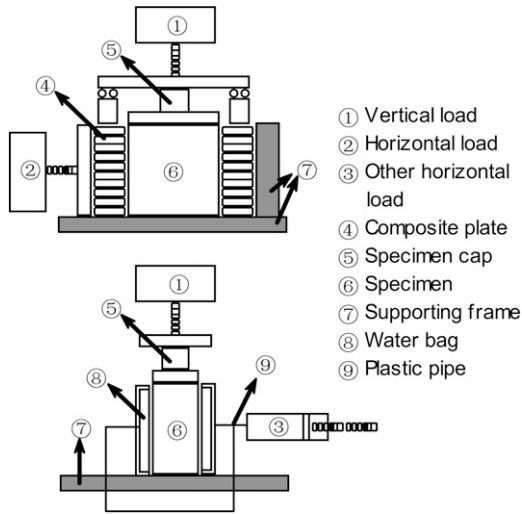


Fig. 2. Diagram of TTA

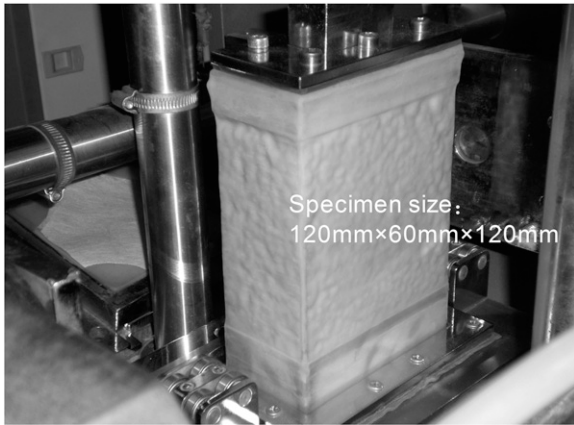


Fig. 3. Specimen installation in TTA

Table 1. Initial State of Specimen

Initial void ratio e_0	Minor principal stress σ_3 (kPa)	b -value
0.26	100	0, 0.25, 0.5, 0.75, 1
0.26	200	0, 0.25, 0.5, 0.75, 1
0.26	300	0, 0.25, 0.5, 0.75, 1
0.26	400	0, 0.25, 0.5, 0.75, 1

Fig. 6 shows the comparisons of the stress-strain, peak friction angle, and maximum dilatancy behaviors of RFMs from triaxial test data (Charles and Watts 1980) and true triaxial test data at $b = 0$ (i.e., the current work). Two RFMs at the same confining pressure (i.e., $\sigma_3 = 100$ kPa) exhibit similar stress-strain behaviors, the same peak friction angle, and the same maximum dilatancy. The comparisons confirm that the true triaxial test results in the current work are valid.

Fig. 7 shows the stress-strain relationships of the RFM in relation to the minor principal stress σ_3 and the b -value. An increase in σ_3 at $b = 0$ leads to a decrease in the stress ratio at the same axial strain [as shown in Fig. 7(a)], but an increase in the volumetric strain at the same axial strain [as shown in Fig. 7(b)]. An increase in the

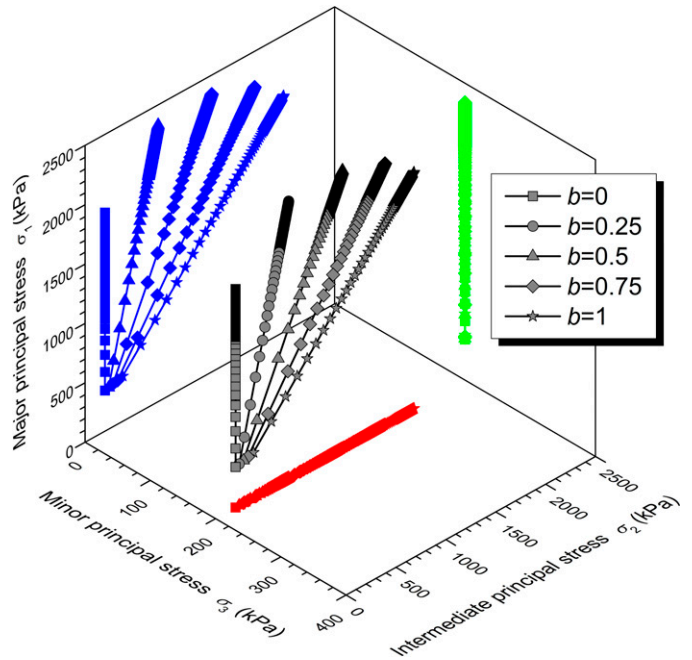


Fig. 4. Stress paths of RFM at $\sigma_3 = 200$ kPa

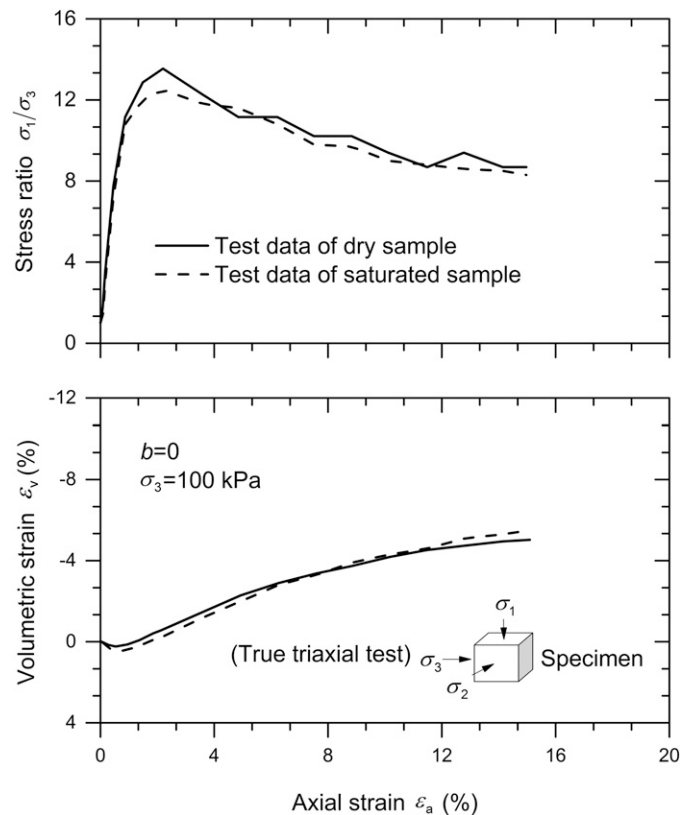


Fig. 5. Comparisons of stress-strain behaviors of RFM under dry condition and drained condition

b -value at $\sigma_3 = 400$ kPa results in a decrease in the stress ratio at the same axial strain [as shown in Fig. 7(c)], but an increase in the volumetric strain at the same axial strain [as shown in Fig. 7(d)]. The test data on the strength and dilatancy of the RFM are analyzed in the following section.

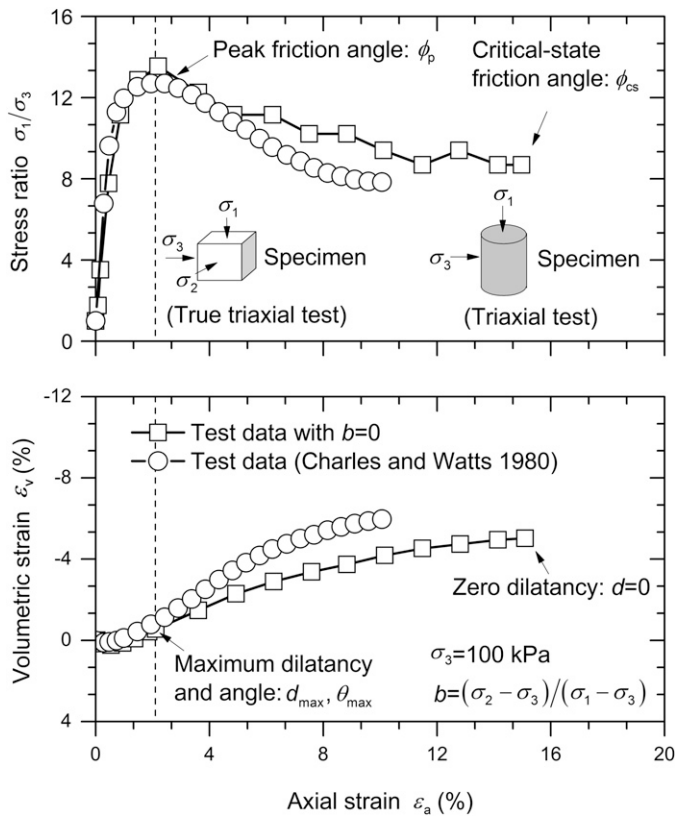


Fig. 6. Comparisons of stress-strain, peak friction angle, and maximum dilatancy of RFM from triaxial test data and true triaxial test data

Data Analyses

Peak Friction Angle

The peak friction angle ϕ_p is defined as the maximum mobilized friction angle ϕ_m during shearing. Fig. 8 shows that the peak friction angle ϕ_p of the RFM depends on the minor principal stress σ_3 (i.e., the initial confining pressure p_0) and the b -value. As shown in Fig. 8(a), the peak friction angle ϕ_p increases to a peak value and then decreases with the b -value. Furthermore, the peak friction angle ϕ_p decreases with an increase in the minor principal stress σ_3 [as shown in Fig. 8(b)].

Critical-State Friction Angle

The critical-state friction angle ϕ_{cs} is defined as the mobilized friction angle ϕ_m at a constant volumetric strain under the drained compression condition. The value of ϕ_{cs} on the RFM in tests is approximate, because the rate of the incremental volumetric strain at the end of the tests is not equal to zero but is within a minimal value. The critical-state friction angle ϕ_{cs} of the RFM (as shown in Fig. 9) varies with σ_3 and the b -value in the same way as that of the peak friction angle ϕ_p (as shown in Fig. 8). The value of ϕ_{cs} is smaller than that of ϕ_p . The critical-state friction angle is therefore dependent on the load path, and this finding is supported by the work of Chakraborty and Salgado (2010). The critical-state friction angle of Toyoura sand with $b = 0.25$ for the plane-strain condition is greater than that with $b = 0$ for the triaxial compression condition (Chakraborty and Salgado 2010). The critical-state friction angle of the RFM with b -value = 0.25 is also greater than that with b -value = 0 [as shown in Fig. 9(a)].

Incremental Friction Angle

The incremental friction angle ($\phi_{inc} = \phi_p - \phi_{cs}$) of the RFM (as shown in Fig. 10) is correlated to the minor principal stress σ_3 and the b -value. An increase in the b -value leads to a decrease in the incremental friction angle ϕ_{inc} [as shown in Fig. 10(a)]. Furthermore, an increase in the minor principal stress σ_3 results in a decrease in the incremental friction angle ϕ_{inc} [as shown in Fig. 10(b)].

Maximum Dilatancy Angle

The maximum dilatancy angle θ_{max} of the RFM at a specified σ_3 decreases with an increase in the b -value [as shown in Fig. 11(a)]. An increase in the minor principal stress σ_3 leads to a decrease in the maximum dilatancy angle θ_{max} of the RFM at a specified b -value [as shown in Fig. 11(b)]. The trend of the maximum dilatancy angle θ_{max} of the RFM depending on the b -value and σ_3 is similar to that of the incremental friction angle ϕ_{inc} . This indicates an intrinsic relationship between the maximum dilatancy angle θ_{max} and the incremental friction angle ϕ_{inc} for the RFM.

Relationship between Incremental Friction Angle and Revised Relative Index

Bolton (1986) found an intrinsic relationship between strength and dilatancy through tests of 17 sands. RFM in a dense state (i.e., at a low confining pressure, as shown in Fig. 6) can exhibit strain-softening behavior and volumetric expansion behavior (i.e., dilatancy). Fig. 6 shows that the axial strain of the peak strength (i.e., the peak friction angle ϕ_p) is the same as that of the maximum dilatancy d_{max} (or the maximum dilatancy angle θ_{max}). The intrinsic relationship between strength and dilatancy can be described by the relative dilatancy index I_R [i.e., Eq. (11) proposed by Bolton (1986)].

A revised relative dilatancy index I_{RR} is suggested by including the atmospheric pressure p_a for the normalization of the pressure units and the parameter $R(b)$ pertaining to the b -value (to incorporate the influence of the b -value on dilatancy and the peak friction angle). The expression of I_{RR} can be given as

$$I_{RR} = I_D [Q - \ln(p'/p_a)] - R(b) \quad (13)$$

The incremental friction angle ϕ_{inc} can be expressed as a linear formulation of the revised relative dilatancy index I_{RR}

$$\phi_{inc} = \alpha_\phi I_{RR} = \alpha_\phi \{ I_D [Q - \ln(p'/p_a)] - R(b) \} \quad (14)$$

where the coefficient α_ϕ = ratio of the incremental friction angle ϕ_{inc} to the revised relative dilatancy index I_{RR} .

The incremental friction angle ϕ_{inc} (as shown in Fig. 12) is linearly correlated to the logarithm of the mean effective stress p'_f at the peak failure state. The linear expression of ϕ_{inc} pertaining to p'_f can be given as

$$\phi_{inc} = \phi_{inc0} - \chi_p \ln(p'_f/p_a) \quad (15)$$

where ϕ_{inc0} = incremental friction angle at the atmospheric pressure; and the coefficient χ_p = gradient of the line of ϕ_{inc0} versus $\ln(p'_f/p_a)$. The values of ϕ_{inc0} and χ_p are listed in Table 2.

Fig. 12 shows that the simulation line of ϕ_{inc0} versus $\ln(p'_f/p_a)$ varies with the b -value. The relative density I_D is kept as a constant of 0.85. The parameter Q in the relative dilatancy index (Bolton 1986) is 10. The value of Q for I_{RR} in Eq. (13) is equal to 5.39, because the

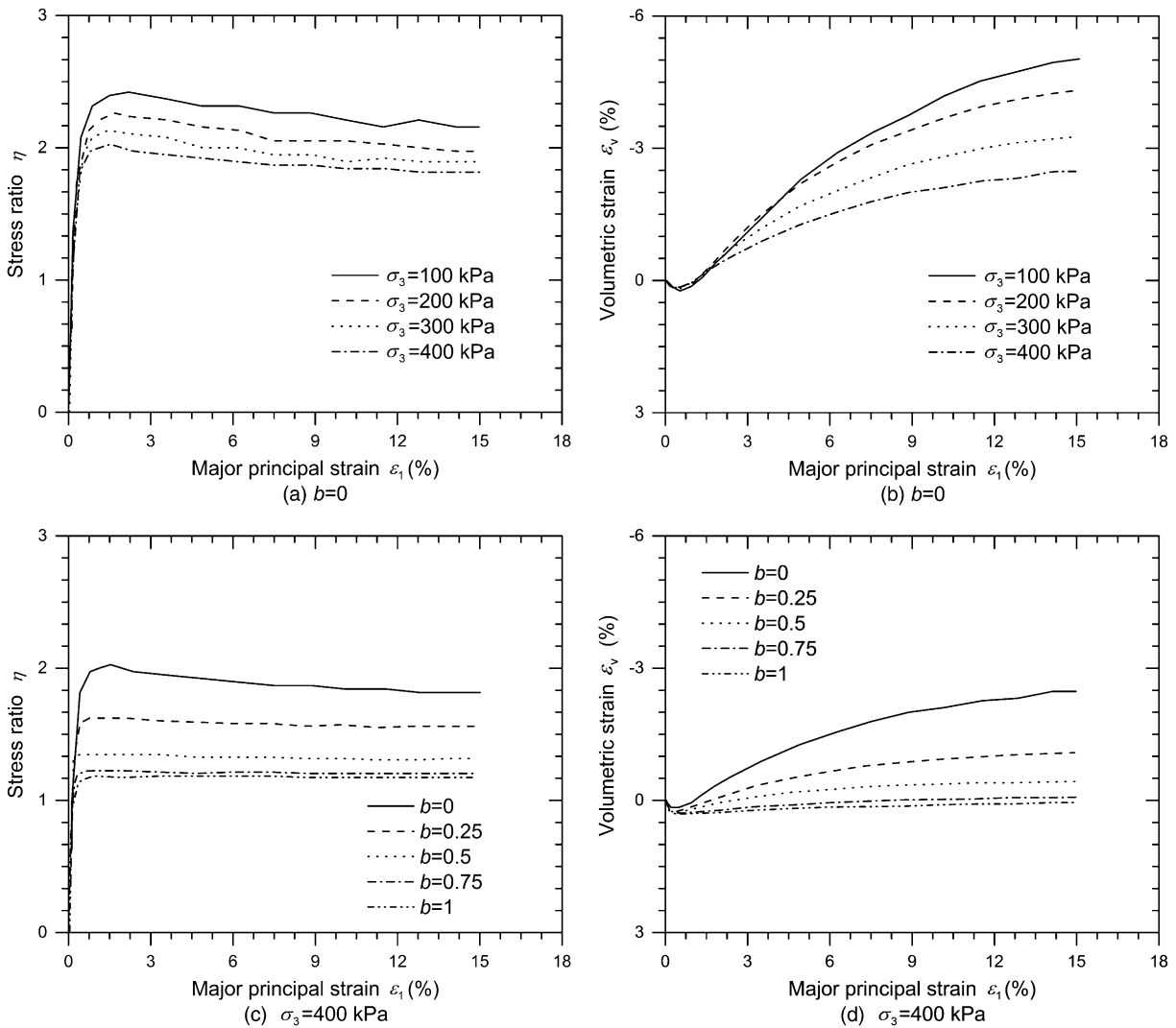


Fig. 7. Stress-strain behaviors of RFM: (a) stress ratio versus major principal strain with change of σ_3 ; (b) volumetric strain versus major principal strain with change of σ_3 ; (c) stress ratio versus major principal strain with change of b -value; (d) volumetric strain versus major principal strain with change of b -value

value of Q (equal to 10) should be subtracted by $\ln p_a$. The combination of Eqs. (14) and (15) gives the values of the parameters α_ϕ and R

$$\alpha_\phi = \chi_p / I_D \quad (16a)$$

$$R(b) = I_D Q - \frac{I_D \phi_{inc0}}{\chi_p} \quad (16b)$$

The parameter $R(b)$ (as shown in Fig. 13) can be simulated by an exponential expression of the b -value. This expression for $R(b)$ can be given as

$$R = R_0 - k_R e^{-k_b b} \quad (17)$$

where R_0 , k_R , and k_b are material constants. The values of R_0 , k_R , and k_b are listed in Table 2.

The revised relative dilatancy index I_{RR} can be obtained by substituting Eq. (17) into Eq. (13)

$$I_{RR} = I_D [Q - \ln(p'/p_a)] - (R_0 + k_R e^{-k_b b}) \quad (18)$$

Substitution of Eq. (18) into Eq. (14) gives

$$\phi_{inc} = \alpha_\phi I_{RR} = \alpha_\phi \{ I_D [Q - \ln(p'/p_a)] - (R_0 + k_R e^{-k_b b}) \} \quad (19)$$

Eq. (19) (as shown in Fig. 14) can capture the variations in ϕ_{inc} with I_{RR} at different b -values.

Fig. 15 shows that the parameter α_ϕ is correlated to the b -value. α_ϕ (as listed in Table 2) is equal to 3.06 at $b = 0$ for the triaxial compression condition. This value of α_ϕ for the RFM is close to 3 for sands (Bolton 1986). For the plane-strain condition, the b -value is assumed to be 0.25 (Chakraborty and Salgado 2010). The α_ϕ value of the RFM at $b = 0.25$ in Table 2 equals 4.94, which is close to 5 for sands (Bolton 1986). As shown in Fig. 15, the parameter α_ϕ in relation to the b -value can be linearly expressed as

$$\alpha_\phi = \alpha_{\phi 0} + k_\alpha b \quad (20)$$

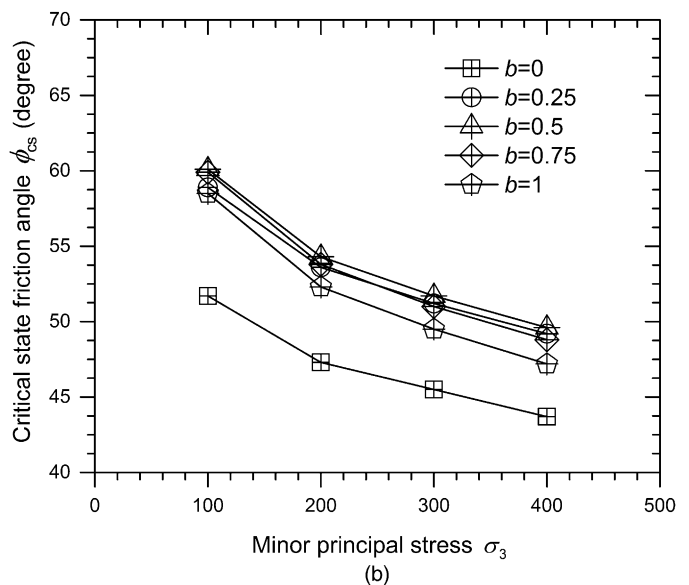
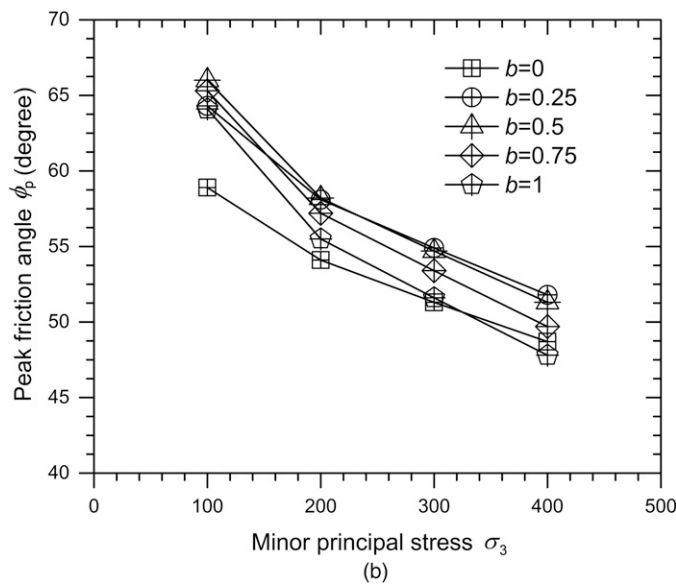
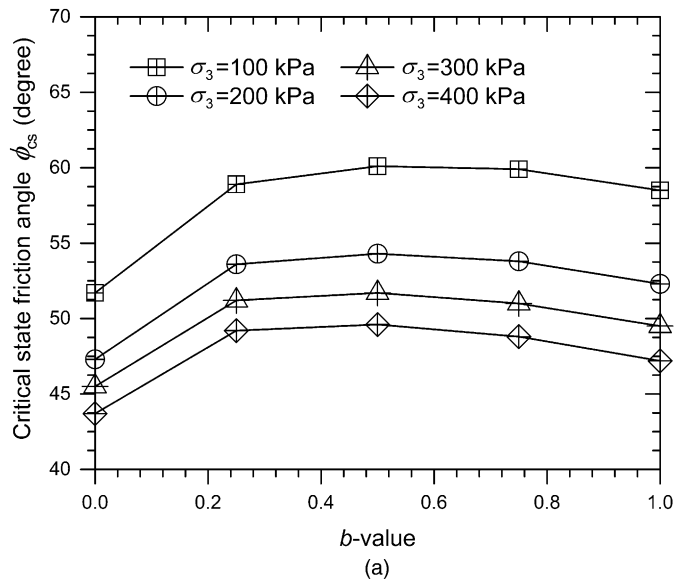
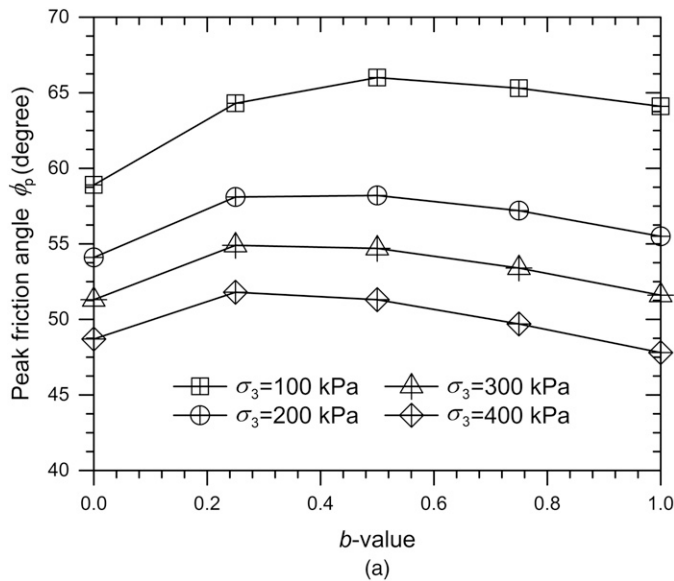


Fig. 8. Variations in peak friction angle of RFM with (a) b -value; (b) minor principal stress

Fig. 9. Variations in critical-state friction angle of RFM with (a) b -value; (b) minor principal stress

where $\alpha_{\phi 0}$ = value of α_{ϕ} at $b = 0$; and k_{α} = gradient of the line of α_{ϕ} versus the b -value. The values of $\alpha_{\phi 0}$ and k_{α} are listed in Table 2. Substitution of Eq. (20) into Eq. (19) gives

$$\phi_{inc} = (\alpha_{\phi 0} + k_{\alpha}b) \left\{ I_D [Q - \ln(p'/p_a)] - (R_0 + k_R e^{-k_b b}) \right\} \quad (21)$$

Fig. 16 shows that the prediction of Eq. (21) agrees well with the test data of the RFM on the incremental friction angle ϕ_{inc} pertaining to the b -value and the revised relative dilatancy index I_{RR} .

Relationship between Incremental Friction Angle and Maximum Dilatancy Angle

The relationship between the incremental friction angle ϕ_{inc} and the maximum dilatancy angle θ_{max} depends on the b -value (as shown in Fig. 17). This relationship can be described by a friction-dilatancy

line with its gradient pertaining to the b -value. Consequently, this relationship can be expressed as

$$\phi_{inc} = \chi_d(b) \theta_{max} \quad (22)$$

where $\chi_d(b)$ in relation to the b -value is the gradient of the friction-dilatancy line. The values of χ_d are listed in Table 2.

Fig. 18 shows that $\chi_d(b)$ pertains linearly to the b -value

$$\chi_d = \chi_{d0} + k_{\chi}b \quad (23)$$

where χ_{d0} = value of χ_d at $b = 0$; and k_{χ} is the gradient of the line of χ_d versus the b -value. The values of χ_{d0} and k_{χ} are listed in Table 2.

Substitution of Eq. (23) into Eq. (22) gives

$$\phi_{inc} = (\chi_{d0} + k_{\chi}b) \theta_{max} \quad (24)$$

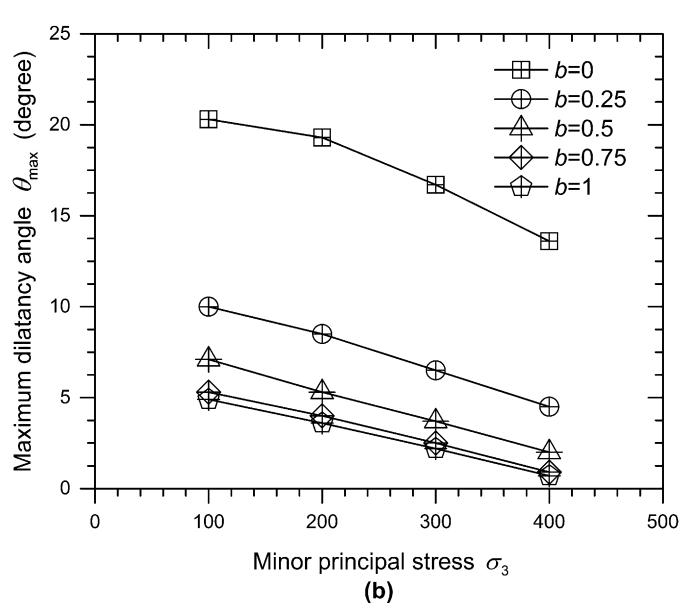
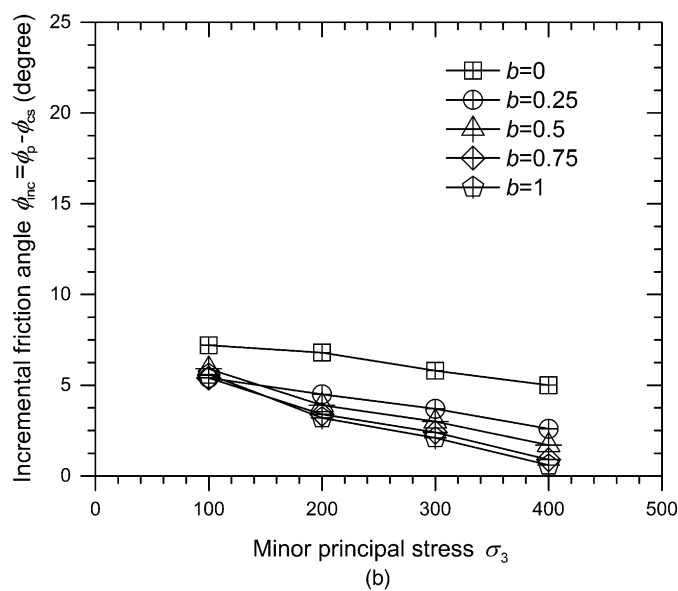
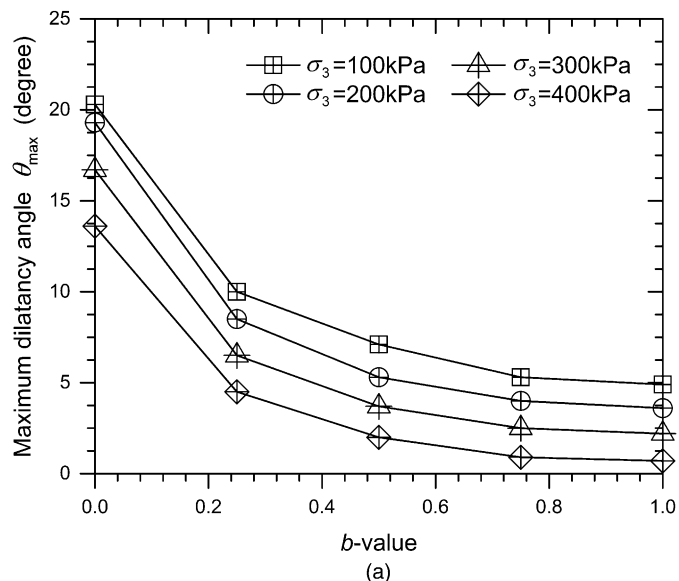
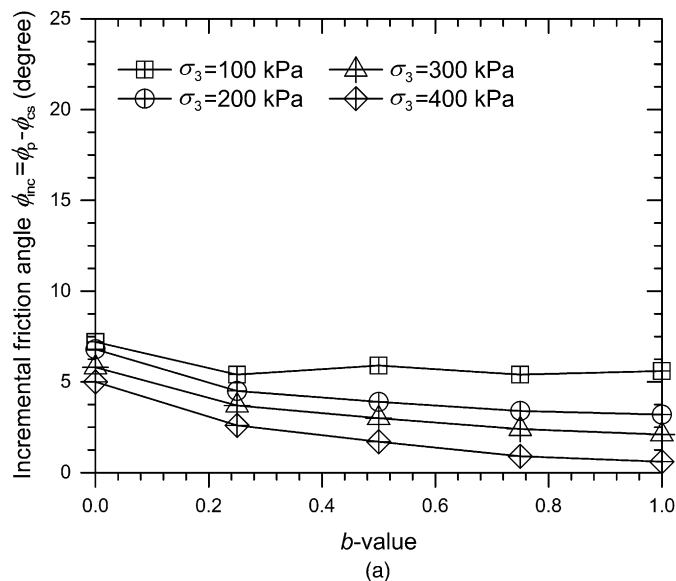


Fig. 10. Variations in incremental friction angle of RFM with (a) b -value; (b) minor principal stress

Fig. 11. Variations in maximum dilatancy angle of RFM with (a) b -value; (b) minor principal stress

The predictions of Eq. (24) are in good agreement with the test data of the RFM on the incremental friction angle ϕ_{inc} pertaining to the b -value and the maximum dilatancy angle θ_{max} (as shown in Fig. 19).

Influence of b -value on Particle Breakage

Experiment results (Lee and Farhoomand 1967; Marsal 1967; Lade et al. 1996; Varadarajan et al. 2003; Coop et al. 2004; Varadarajan et al. 2006) and numerical simulations (Lobo-Guerrero and Vallejo 2005, 2006; Lobo-Guerrero et al. 2006) show that the mechanical behaviors of granular soils are greatly influenced by particle breakage. The RFM in the tests at $\sigma_3 = 100, 200,$ and 300 kPa undergoes marginal particle crushing. This can be attributed mainly to (1) the comparatively low pressure, (2) the rounded shape of the particle, and (3) the high strength of the particle. The RFM at

$\sigma_3 = 400$ kPa produces some particle breakage. However, the influence of particle breakage on the mechanical behaviors of the RFM (e.g., the friction angle) is difficult to analyze, because only the data at $\sigma_3 = 400$ kPa are available. In contrast, the influence of the b -value on the particle breakage of the RFM can be investigated, based on the data at $b = 0, 0.25, 0.5, 0.75,$ and 1 .

The particle size distributions (PSDs) before and after testing are shown in Fig. 20. An increase in the b -value can lead to an increase in the discrepancy of the PSDs before and after testing. The relative breakage index proposed by Hardin (1985) (Fig. 21) was adopted to quantitatively identify the degree of particle breakage for the RFM

$$B_r = \frac{B_l}{B_p} \quad (25)$$

where B_r = relative breakage index; the breakage potential B_p is equal to the area between the vertical line (defining the upper limit of

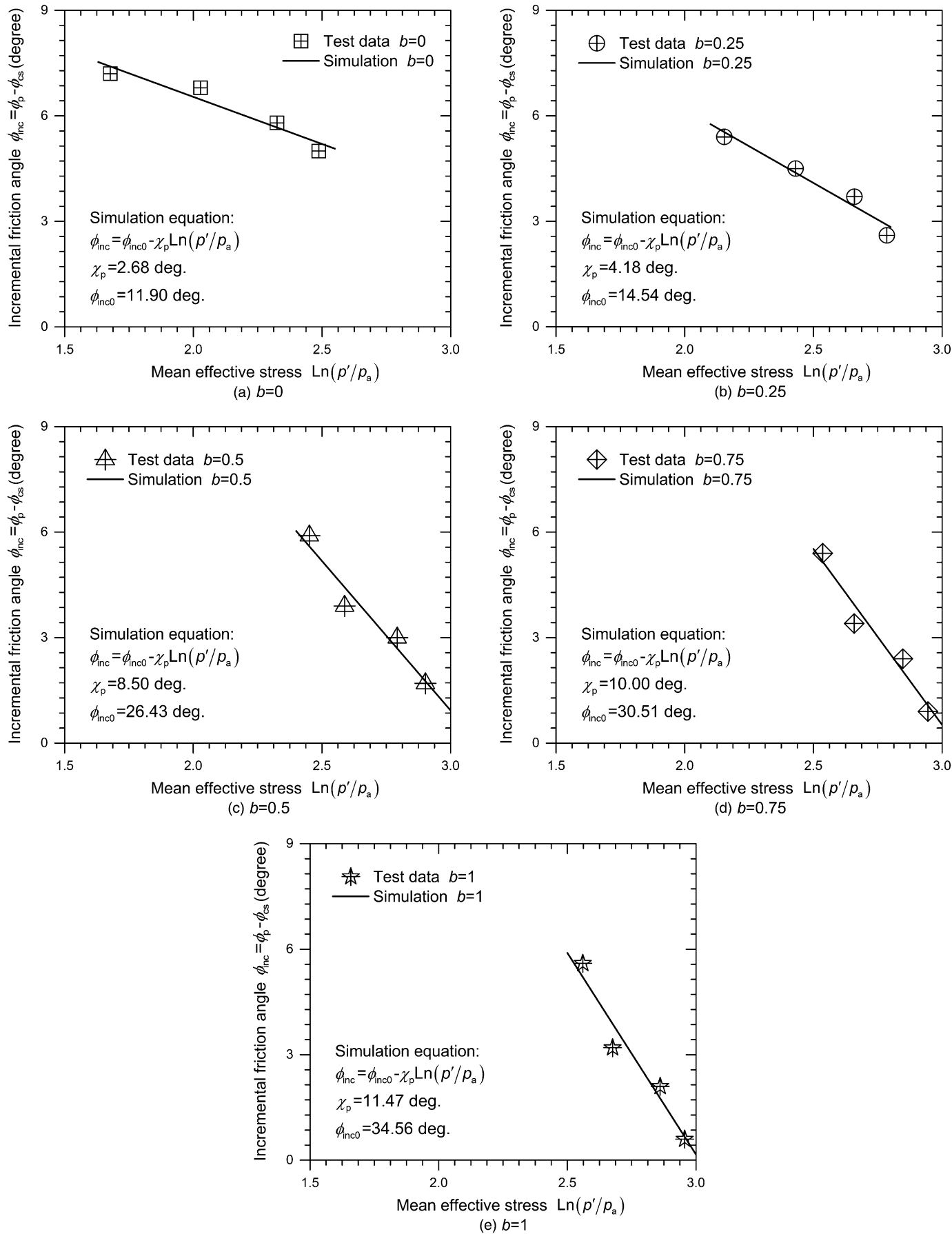


Fig. 12. Simulations for incremental friction angle versus mean effective stress: (a) $b = 0$; (b) $b = 0.25$; (c) $b = 0.5$; (d) $b = 0.75$; (e) $b = 1$

Table 2. Values of Material Constants from Simulation Equations

Equation number	Symbol	Value
Eq. (13)	Q	5.39
Eq. (15)	χ_p	2.68 ^{oa}
		4.18 ^{ob}
		8.50 ^{oc}
		10.00 ^{od}
		11.47 ^{oe}
	ϕ_{inc0}	11.90 ^{oa}
		14.54 ^{ob}
		26.43 ^{oc}
		30.51 ^{od}
		34.56 ^{oe}
Eq. (17)	R_0	2.03
	k_R	1.34
	k_b	5.01
Eq. (20)	$\alpha_{\phi0}$	3.11
	k_α	11.07
Eq. (22)	χ_d	0.35 ^a
		0.55 ^b
		0.80 ^c
		0.96 ^d
		1.04 ^e
Eq. (23)	χ_{d0}	0.38
	k_χ	0.72
Eq. (26)	B_{r0}	5.75
	χ_B	3.75
	k_B	1.61

^aFor $b = 0$.

^bFor $b = 0.25$.

^cFor $b = 0.5$.

^dFor $b = 0.75$.

^eFor $b = 1$.

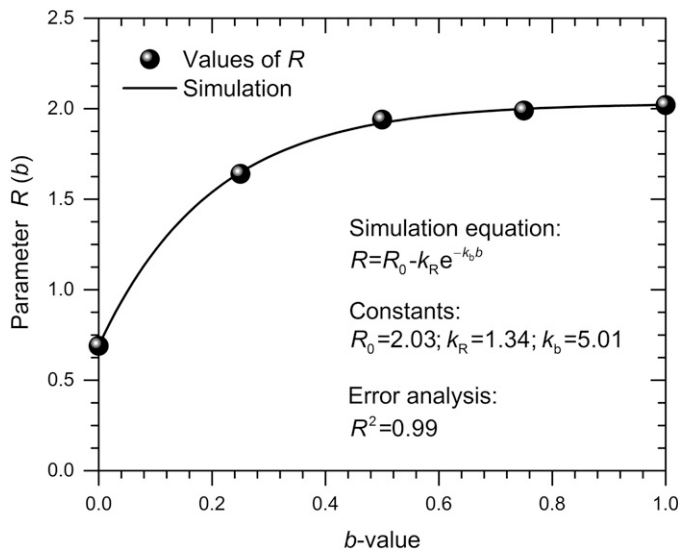


Fig. 13. Variation in parameter R with b -value

the silt size with $d_m = 0.074$ mm) and the initial grading (IG); and the total breakage B_t is equal to the area between the current grading (CG) and the IG. The value of the relative breakage B_r ranges from 0 to 1.

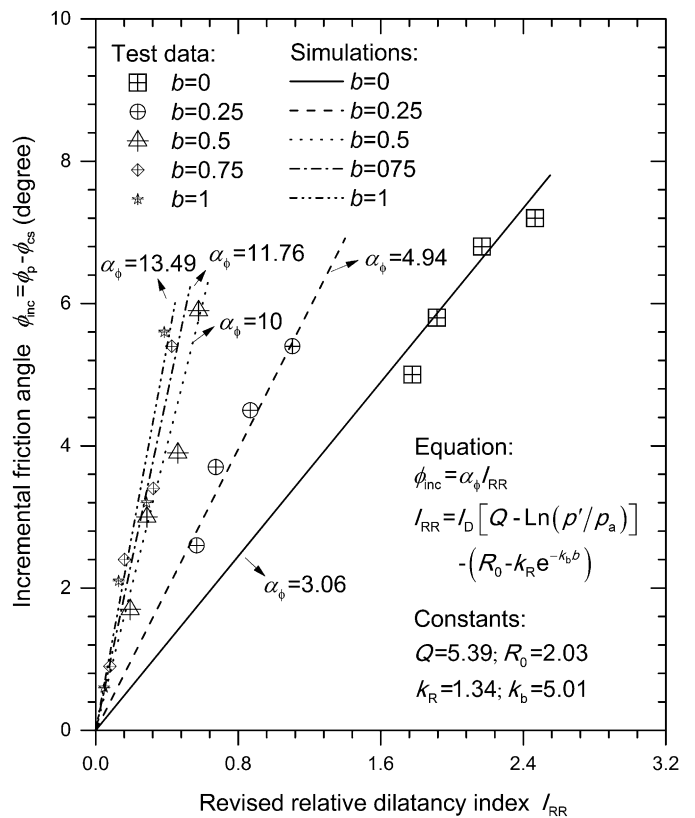


Fig. 14. Comparisons between test data and simulations on relationship between incremental friction angle and revised relative dilatancy index

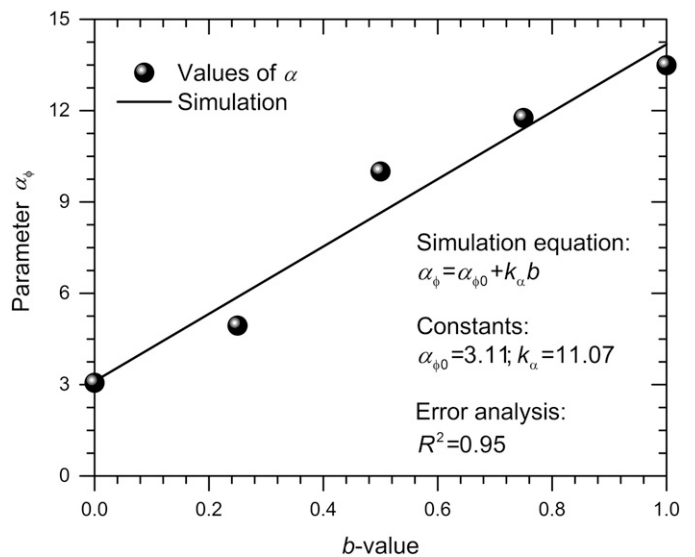


Fig. 15. Relationship between parameter α_ϕ and b -value

An increase in the b -value can result in an increase in particle breakage (as shown in Fig. 22). Therefore, the b -value can influence the particle breakage of the RFM, indicating that the particle breakage of the RFM depends on the stress path. The relationship between the b -value and the relative breakage index B_r can be given as

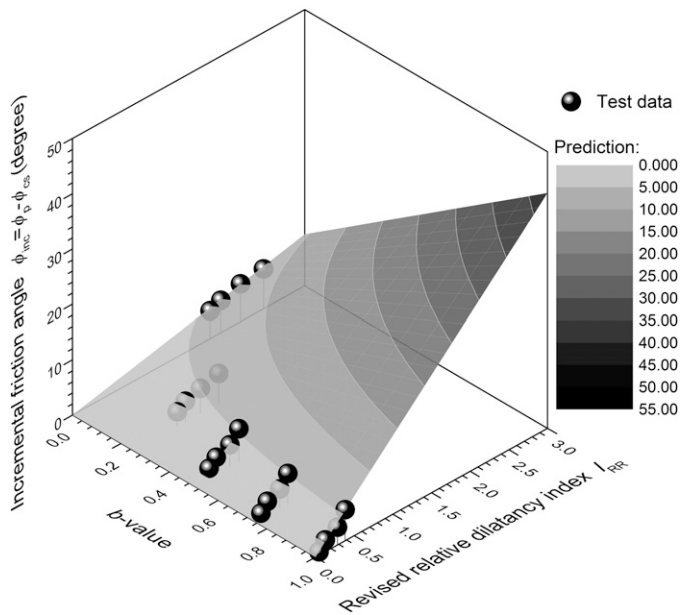


Fig. 16. Predictions of incremental friction angle in relation to revised relative dilatancy index and b -value

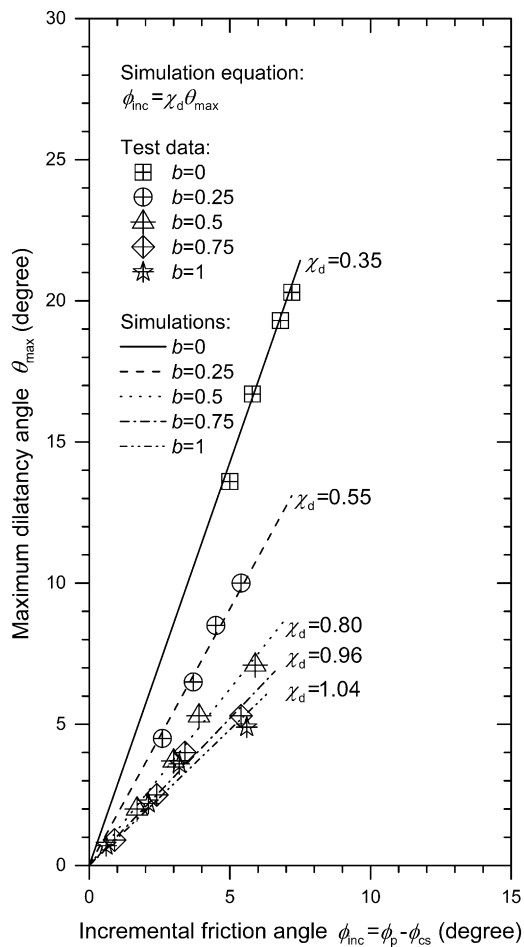


Fig. 17. Simulations and test data on relationship between incremental friction angle and maximum dilatancy angle for different b -values

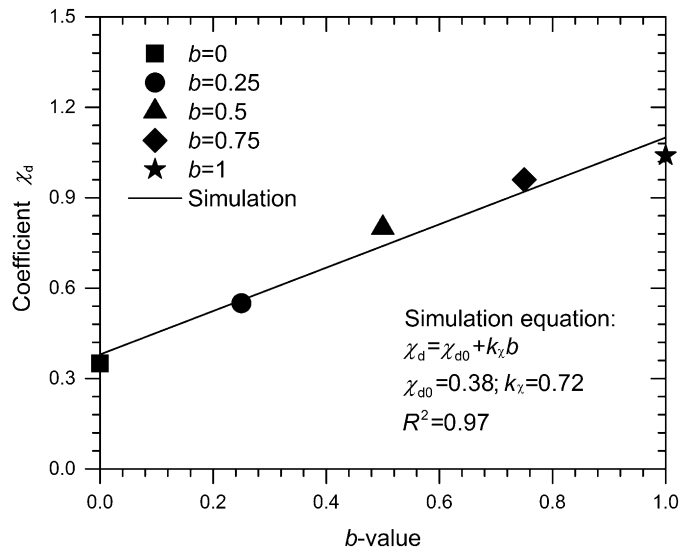


Fig. 18. Relationship between coefficient χ_d and b -value

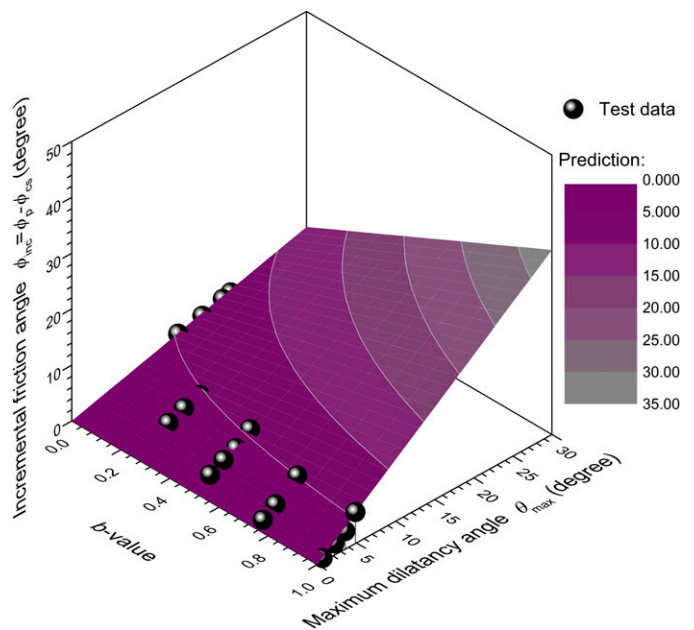


Fig. 19. Predictions of incremental friction angle pertaining to maximum dilatancy angle and b -value

$$B_r = B_{r0} - \chi_B e^{-k_B b} \quad (26)$$

where B_{r0} , χ_B , and k_B are material constants. The values of these material constants are listed in Table 2.

Discussion

The strength and dilatancy of the RFM in general stress paths are investigated through a series of true triaxial compression tests with a constant b -value and confining pressure. The relative dilatancy index was revised to incorporate the effect of the b -value on the stress-dilatancy behaviors of the RFM. The incremental friction angle of the RFM could be expressed by a linear function

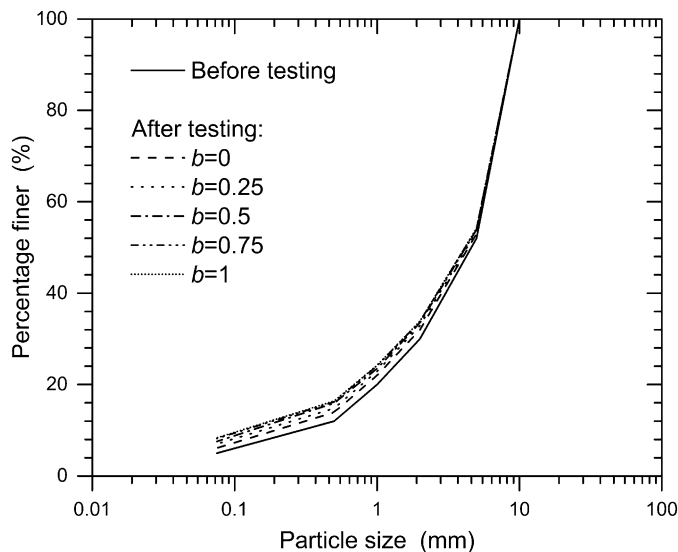


Fig. 20. Particle size distributions before and after testing of RFM at $\sigma_3 = 400$ kPa

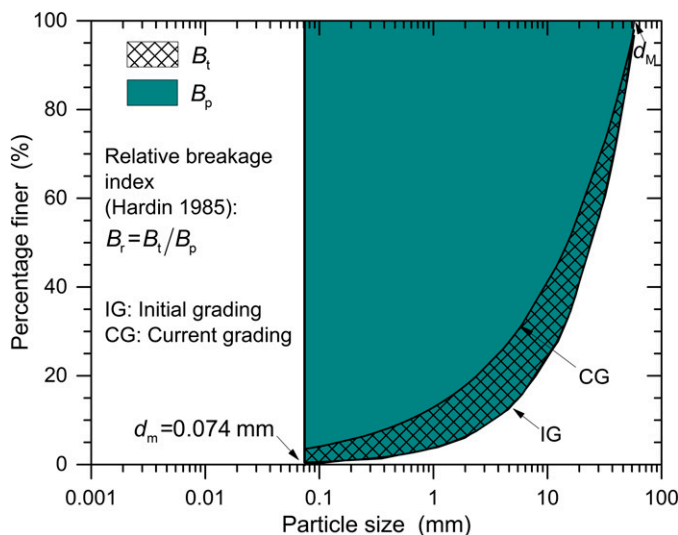


Fig. 21. Definition of Hardin's relative breakage index

[i.e., Eq. (21)] of the revised relative dilatancy index with its gradient in relation to the b -value. Furthermore, a linear formulation [i.e., Eq. (24)] with the coefficient in relation to the b -value can be used to describe the relationship between the incremental friction angle and the maximum dilatancy angle of the RFM. The proposed strength-dilatancy relationships could be applied to evaluate the stability of the slope of rockfill dams in a three-dimensional stress space.

The simulations (as shown in Figs. 12 and 14–16) are not very accurate in comparison with the test data on the incremental friction angles pertaining to the b -value and the revised relative dilatancy index I_{RR} . In contrast, the simulations (as shown in Figs. 18 and 19) are in good agreement with the test data on the incremental friction angles in relation to the b -value and the maximum dilatancy angle θ_{max} . The differential simulations on the incremental friction angles

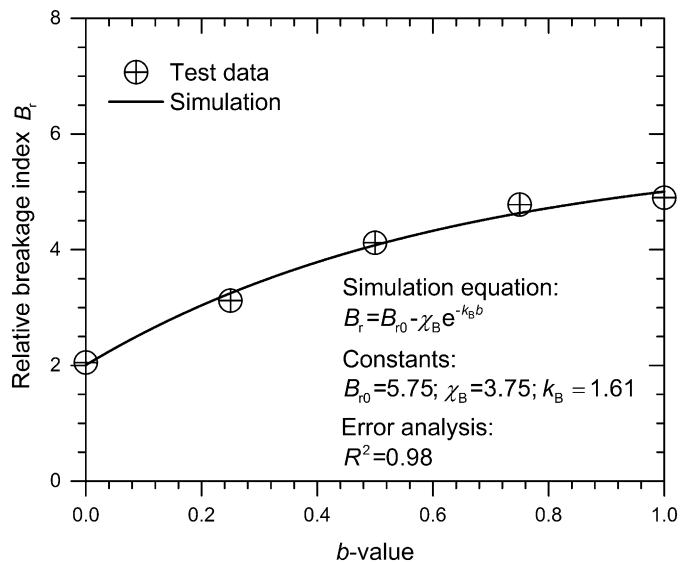


Fig. 22. Influence of b -value on relative breakage index of RFM

are mainly a result of the different definitions of the revised relative dilatancy index I_{RR} and the maximum dilatancy angle θ_{max} . The dilatancy index I_R [proposed by Bolton (1986)] was derived in a two-dimensional space, whereas the maximum dilatancy angle θ_{max} was defined in a three-dimensional space (Yang and Li 2004). The test data of the RFM in the current study were three-dimensional. The revised relative dilatancy index I_{RR} [incorporating the effects of the b -value into the parameter R and the parameter α_ϕ in Eq. (21)] still could not precisely cover all the test data. Although the revised relative dilatancy index could be used to estimate the overall trends of the incremental friction angle of the RFM in general stress paths, a more appropriate and reasonable dilatancy index should be proposed to incorporate the effect of the b -value in future research.

The proposed equations [e.g., Eq. (21) for the relationship between ϕ_p and I_{RR} , Eq. (24) for the relationship between ϕ_p and θ_{max} , and Eq. (26) for the relationship between B_r and the b -value] are only suitable for RFMs possessing stress-strain, strength, and dilatancy behaviors similar to those of the RFM in the current study. Furthermore, the material constants may be changed because of the material properties (e.g., the particle strength, the particle size, and the particle shape).

The maximum particle size of the RFM in this paper was 10 mm, whereas the maximum particle size of the RFM in rockfill dams can be larger than 300 mm, even up to 1,000 mm (Frossard et al. 2012). Based on the ratio of the specimen size to the particle size (ASTM 2002), a specimen size (for a representative 0- to 500-mm rockfill) should be 3,000 mm in diameter and 6,000 mm in height. This specimen weighs more than 80 t. The construction of apparatus for such a specimen would be not only highly expensive but also technically impossible. The strength and deformation of RFMs depend on the maximum particle size (Indraratna et al. 1993; Varadarajan et al. 1997, 1999; Gupta 2000; Varadarajan et al. 2002, 2003, 2006; Gupta 2009a, b; Honkanadavar and Gupta 2010; Seif El Dine et al. 2010; Abbas 2011; Honkanadavar et al. 2011, 2012; Vasistha et al. 2012; Honkanadavar and Sharma 2013; Vasistha et al. 2013). Smaller aggregates contain fewer cracks and defects, and typically exhibit higher strengths in comparison with prototype rockfill-size materials (Billam 1971; McDowell et al. 1996; McDowell and Bolton 1998). The mechanical behavior of the finer-grained granular material would be different from that of the

coarse-grained granular material with the same mineral. Therefore, the strength and dilatancy behavior of the 0- to 10-mm RFM in this paper would be different from that of the prototype RFM.

Frossard et al. (2012) proposed an original method (i.e., a general size-effect relation based on fracture mechanics) for evaluating the shear strength of such material. This method makes it possible to evaluate the shear strength of a coarse-grained granular material from the measured properties of a finer-grained granular material with the same mineral. This method (Frossard et al. 2012) can possibly be used to evaluate the mechanical behaviors of the prototype RFM, based on the true triaxial tests of the 0- to 10-mm RFM in this paper. Details about this work are introduced in Xiao et al. (2014c).

Conclusions

In this paper, a series of true triaxial compression tests on RFMs was carried out to investigate variations in the peak friction angle, critical-state friction angle, incremental friction angle, and maximum dilatancy angle with the initial confining pressures and the b -value. The main conclusions are summarized as follows:

1. The peak friction angle and critical-state friction angle of the RFM at a specified σ_3 increased to a peak value and then decreased with an increase in the b -value. The peak friction angle and critical-state friction angle of the RFM at a specified b -value decreased with an increase in σ_3 . The incremental friction angle and the maximum dilatancy angle of the RFM decreased with an increase in the b -value at a specified σ_3 , or decreased with an increase in σ_3 at a specified b -value.
2. A revised relative dilatancy index was proposed to capture the variation in the incremental friction angle of the RFM with the b -value. The incremental friction angle of the RFM could be expressed by a linear function of the revised relative dilatancy index with its gradient pertaining to the b -value. The proposed equation could predict well the test data in terms of a relationship among the incremental friction angle, the revised relative dilatancy index, and the b -value.
3. The relationship between the incremental friction angle and the maximum dilatancy angle of the RFM depended on the b -value. This relationship could be simulated by a linear formulation with its gradient pertaining to the b -value. The predictions by the proposed formulation agreed well with the test data in terms of a relationship among the incremental friction angle, the maximum dilatancy angle, and the b -value.
4. An increase in the b -value for the RFM at $\sigma_3 = 400$ kPa could result in an increase in particle breakage. Therefore, the b -value could influence the particle breakage of the RFM, indicating that the particle breakage of the RFM depends on the stress path.

Acknowledgments

The authors acknowledge the financial support of the 111 Project (Grant No. B13024), the Program for Changjiang Scholars and Innovative Research Team in University (Grant No. IRT1125), and the Fundamental Research Funds for the Central Universities (Grant No. 2011B14514). The authors also thank Dr. J. He and Dr. W. G. Zhang (at the School of Civil and Environmental Engineering, Nanyang Technological University) for their review of the language.

Notation

The following symbols are used in this paper:

- B_p = breakage potential;
- B_r = relative breakage index;
- B_{r0} = material constant in relation to particle breakage;
- B_t = total breakage;
- b = intermediate principal stress ratio;
- C_c = curvature coefficient;
- C_u = uniformity coefficient;
- d = dilatancy;
- $d\epsilon_s$ = increment of shear strain;
- $d\epsilon_v$ = increment of volumetric strain;
- e = void ratio;
- e_{\max} = maximum void ratio;
- e_{\min} = minimum void ratio;
- e_0 = initial void ratio;
- I_D = initial relative density;
- I_R = relative dilatancy index;
- I_{RR} = revised relative dilatancy index;
- k_B = material constant in relation to particle breakage;
- k_b = material constant related to R ;
- k_R = material constant related to R ;
- k_{α} = gradient of line of α_ϕ versus b -value;
- k_{χ} = gradient of line of χ_d versus b -value;
- p' = mean effective stress;
- p_a = atmospheric pressure;
- p'_f = mean effective stress at failure state;
- p_0 = initial confining pressure;
- Q = state index constant of material;
- q = deviatoric stress;
- R = state index constant of material;
- R_0 = material constant related to R ;
- α_ϕ = ratio of incremental friction angle ϕ_{inc} to revised state index I_{RR} ;
- $\alpha_{\phi 0}$ = value of α_ϕ with $b = 0$;
- ϵ_1 = major principal strain;
- ϵ_2 = intermediate principal strain;
- ϵ_3 = minor principal strain;
- η = stress ratio;
- η_p = peak stress ratio;
- θ_{\max} = maximum dilatancy angle;
- σ_1 = major effective principal stress;
- σ_2 = intermediate effective principal stress;
- σ_3 = minor effective principal stress;
- ϕ_{cs} = critical-state friction angle;
- ϕ_{inc} = incremental friction angle;
- $\phi_{\text{inc}0}$ = incremental friction angle at atmospheric pressure;
- ϕ_m = mobilized friction angle;
- ϕ_p = peak friction angle;
- χ_B = material constant in relation to particle breakage;
- χ_d = ratio of incremental friction angle ϕ_{inc} versus maximum dilatancy angle θ_{\max} ;
- χ_{d0} = value of χ_d with $b = 0$; and
- χ_p = gradient of line of ϕ_{inc} versus logarithm of p'_f/p_a .

References

- Abbas, S. M. (2011). *Constitutive modeling of rockfill materials*, Lambert Academic Publishing, Saarbrücken, Germany.

- Agustian, A., and Goto, S. (2008). "Strength and deformation characteristics of scoria in triaxial compression at low confining stress." *Soils Found.*, 48(1), 27–39.
- Anderson, W. F., and Fair, P. (2008). "Behavior of railroad ballast under monotonic and cyclic loading." *J. Geotech. Geoenviron. Eng.*, 10.1061/(ASCE)1090-0241(2008)134:3(316), 316–327.
- ASTM. (2002). "Standard test method for consolidated undrained triaxial compression test for cohesive soils." *D4767-04*, West Conshohocken, PA.
- ASTM. (2010). "Standard test method for compressive strength and elastic moduli of intact rock core specimens under varying states of stress and temperatures." *D7012-10*, West Conshohocken, PA.
- ASTM. (2014). "Advanced triaxial testing of soil and rock." *STP977-88*, West Conshohocken, PA.
- Billam, J. (1971). "Some aspects of the behaviour of granular materials at high pressure." *Proc., Roscoe Memorial Symp. on Stress-Strain Behaviour of Soils*, Foulis, Henley, U.K., 69–80.
- Bolton, M. D. (1986). "The strength and dilatancy of sands." *Géotechnique*, 36(1), 65–78.
- Chakraborty, T., and Salgado, R. (2010). "Dilatancy and shear strength of sand at low confining pressures." *J. Geotech. Geoenviron. Eng.*, 10.1061/(ASCE)GT.1943-5606.0000237, 527–532.
- Charles, J. A. (1975). "Strains developed in two rockfill dams during construction." *Géotechnique*, 25(2), 321–332.
- Charles, J. A., and Watts, K. S. (1980). "The influence of confining pressure on the shear strength of compacted rockfill." *Géotechnique*, 30(4), 353–367.
- Chu, J., Lo, S.-C. R., and Lee, I. K. (1996). "Strain softening and shear band formation of sand in multi-axial testing." *Géotechnique*, 46(1), 63–82.
- Coop, M. R., Sorensen, K. K., Bodas Freitas, T., and Georgoutsos, G. (2004). "Particle breakage during shearing of a carbonate sand." *Géotechnique*, 54(3), 157–163.
- Daouadj, A., and Hicher, P.-Y. (2010). "An enhanced constitutive model for crushable granular materials." *Int. J. Numer. Anal. Methods Geomech.*, 34(6), 555–580.
- Desai, C. S., and El-Hoseiny, K. E. (2005). "Prediction of field behavior of reinforced soil wall using advanced constitutive model." *J. Geotech. Geoenviron. Eng.*, 10.1061/(ASCE)1090-0241(2005)131:6(729), 729–739.
- Desai, C. S., and Faruque, M. O. (1984). "Constitutive model for (geological) materials." *J. Eng. Mech.*, 10.1061/(ASCE)0733-9399(1984)110:9(1391), 1391–1408.
- Desai, C. S., Jagannath, S. V., and Kundu, T. (1995). "Mechanical and ultrasonic anisotropic response of soil." *J. Eng. Mech.*, 10.1061/(ASCE)0733-9399(1995)121:6(744), 744–752.
- Desai, C. S., Janardhanam, R., and Sture, S. (1982). "High capacity multiaxial testing device." *Geotech. Test. J.*, 5(1/2), 26–33.
- Desai, C. S., and Salami, M. R. (1987). "Constitutive model for rocks." *J. Geotech. Eng.*, 10.1061/(ASCE)0733-9410(1987)113:5(407), 407–423.
- Desai, C. S., and Toth, J. (1996). "Disturbed state constitutive modeling based on stress-strain and nondestructive behavior." *Int. J. Solids Struct.*, 33(11), 1619–1650.
- European Committee for Standardization (CEN). (2010). "Tests for mechanical and physical properties of aggregates. Methods for the determination of resistance to fragmentation." *EN 1097-2*, Brussels, Belgium.
- Frossard, E., Hu, W., Dano, C., and Hicher, P.-Y. (2012). "Rockfill shear strength evaluation: A rational method based on size effects." *Géotechnique*, 62(5), 415–427.
- Fu, Z., Chen, S., and Peng, C. (2013). "Modeling cyclic behavior of rockfill materials in a framework of generalized plasticity." *Int. J. Geomech.*, 10.1061/(ASCE)GM.1943-5622.0000302, 191–204.
- Gupta, A. K. (2000). "Constitutive modeling of rockfill materials." Ph.D. thesis, Indian Institute of Technology, Delhi, India.
- Gupta, A. K. (2009a). "Effect of particle size and confining pressure on breakage and strength parameters of rockfill materials." *Electron. J. Geotech. Eng.*, 14(H), 1–12.
- Gupta, A. K. (2009b). "Triaxial behaviour of rockfill materials." *Electron. J. Geotech. Eng.*, 14(J), 1–18.
- Hardin, B. O. (1985). "Crushing of soil particles." *J. Geotech. Engrg.*, 10.1061/(ASCE)0733-9410(1985)111:10(1177), 1177–1192.
- Honkanadavar, N. P., and Gupta, S. L. (2010). "Prediction of shear strength parameters for prototype riverbed rockfill material using index properties." *Proc., Indian Geotechnical Conf.*, Indian Geotechnical Society, New Delhi, India, 335–338.
- Honkanadavar, N. P., Gupta, S. L., and Bajaj, S. (2011). "Deformability characteristics of quarried rockfill material." *Int. J. Earth Sci. Eng.*, 4(6), 128–131.
- Honkanadavar, N. P., Gupta, S. L., and Ratnam, M. (2012). "Effect of particle size and confining pressure on shear strength parameter of rockfill materials." *Int. J. Adv. Civ. Eng. Archit.*, 1(1), 49–63.
- Honkanadavar, N. P., and Sharma, K. G. (2013). "Testing and modeling the behavior of riverbed and blasted quarried rockfill materials." *Int. J. Geomech.*, 10.1061/(ASCE)GM.1943-5622.0000378, 04014028.
- Indraratna, B., Ionescu, D., and Christie, H. D. (1998). "Shear behavior of railway ballast based on large-scale triaxial tests." *J. Geotech. Geoenviron. Eng.*, 10.1061/(ASCE)1090-0241(1998)124:5(439), 439–449.
- Indraratna, B., Wijewardena, L. S. S., and Balasubramaniam, A. S. (1993). "Large-scale triaxial testing of grey wacke rockfill." *Géotechnique*, 43(1), 37–51.
- Janardhanam, R., and Desai, C. S. (1983). "Three-dimensional testing and modeling of ballast." *J. Geotech. Engrg.*, 10.1061/(ASCE)0733-9410(1983)109:6(783), 783–796.
- Kohgo, Y., Asano, I., and Hayashida, Y. (2007). "Mechanical properties of unsaturated low quality rockfills." *Soils Found.*, 47(5), 947–959.
- Lackenby, J., Indraratna, B., McDowell, G., and Christie, D. (2007). "Effect of confining pressure on ballast degradation and deformation under cyclic triaxial loading." *Géotechnique*, 57(6), 527–536.
- Lade, P. V., Yamamuro, J. A., and Bopp, P. A. (1996). "Significance of particle crushing in granular materials." *J. Geotech. Engrg.*, 10.1061/(ASCE)0733-9410(1996)122:4(309), 309–316.
- Lashkari, A. (2009). "On the modeling of the state dependency of granular soils." *Comput. Geotech.*, 36(7), 1237–1245.
- Lee, K. L., and Farhoomand, I. (1967). "Compressibility and crushing of granular soil in anisotropic triaxial compression." *Can. Geotech. J.*, 4(1), 68–86.
- Leps, T. M. (1970). "Review of shearing strength of rockfill." *J. Soil Mech. and Found. Div.*, 96(4), 1159–1170.
- Lobo-Guerrero, S., and Vallejo, L. E. (2005). "Analysis of crushing of granular material under isotropic and biaxial stress conditions." *Soils Found.*, 45(4), 79–87.
- Lobo-Guerrero, S., and Vallejo, L. E. (2006). "Discrete element method analysis of railtrack ballast degradation during cyclic loading." *Granul. Matter*, 8(3–4), 195–204.
- Lobo-Guerrero, S., Vallejo, L. E., and Vesga, L. F. (2006). "Visualization of crushing evolution in granular materials under compression using DEM." *Int. J. Geomech.*, 10.1061/(ASCE)1532-3641(2006)6:3(195), 195–200.
- Lowe, J. (1964). "Shear strength of coarse embankment dam materials." *Proc., 8th Int. Congress on Large Dams*, International Commission on Large Dams, Paris, 745–761.
- Marsal, R. J. (1967). "Large-scale testing of rockfill materials." *J. Soil Mech. and Found. Div.*, 93(2), 27–43.
- Marschi, N. D., Chan, C. K., and Seed, H. B. (1972). "Evaluation of properties of rockfill materials." *J. Soil Mech. and Found. Div.*, 98(1), 95–114.
- Matheson, G. M. (1986). "Relationship between compacted rockfill density and gradation." *J. Geotech. Engrg.*, 10.1061/(ASCE)0733-9410(1986)112:12(1119), 1119–1124.
- McDowell, G. R., and Bolton, M. D. (1998). "On the micromechanics of crushable aggregates." *Géotechnique*, 48(5), 667–679.
- McDowell, G. R., Bolton, M. D., and Robertson, D. (1996). "The fractal crushing of granular materials." *J. Mech. Phys. Solids*, 44(12), 2079–2101.
- Oldecop, L. A., and Alonso, E. E. (2001). "A model for rockfill compressibility." *Géotechnique*, 51(2), 127–139.
- Salgado, R., Bandini, P., and Karim, A. (2000). "Shear strength and stiffness of silty sand." *J. Geotech. Geoenviron. Eng.*, 10.1061/(ASCE)1090-0241(2000)126:5(451), 451–462.

- Salgado, R., Boulanger, R. W., and Mitchell, J. K. (1997a). "Lateral stress effects on CPT liquefaction resistance correlations." *J. Geotech. Geoenviron. Eng.*, 10.1061/(ASCE)1090-0241(1997)123:8(726), 726–735.
- Salgado, R., Mitchell, J. K., and Jamiolkowski, M. (1997b). "Cavity expansion and penetration resistance in sand." *J. Geotech. Geoenviron. Eng.*, 10.1061/(ASCE)1090-0241(1997)123:4(344), 344–354.
- Salgado, R., Mitchell, J. K., and Jamiolkowski, M. (1998). "Calibration chamber size effects on penetration resistance in sand." *J. Geotech. Geoenviron. Eng.*, 10.1061/(ASCE)1090-0241(1998)124:9(878), 878–888.
- Salgado, R., and Randolph, M. F. (2001). "Analysis of cavity expansion in sand." *Int. J. Geomech.*, 10.1061/(ASCE)1532-3641(2001)1:2(175), 175–192.
- Seif El Dine, B., Dupla, J. C., Frank, R., Canou, J., and Kazan, Y. (2010). "Mechanical characterization of matrix coarse-grained soils with a large-sized triaxial device." *Can. Geotech. J.*, 47(4), 425–438.
- Sevi, A., and Ge, L. (2012). "Cyclic behaviors of railroad ballast within the parallel gradation scaling framework." *J. Mater. Civ. Eng.*, 10.1061/(ASCE)MT.1943-5533.0000460, 797–804.
- Shi, W. C. (2008). "True triaxial tests on coarse-grained soils and study on constitutive model." Ph.D. thesis, Hohai Univ., Nanjing, China.
- Vaid, Y. P., and Sasitharan, S. (1992). "The strength and dilatancy of sand." *Can. Geotech. J.*, 29(3), 522–526.
- Varadarajan, A., Sharma, K. G., Abbas, S. M., and Dhawan, A. K. (2006). "Constitutive model for rockfill materials and determination of material constants." *Int. J. Geomech.*, 10.1061/(ASCE)1532-3641(2006)6:4(226), 226–237.
- Varadarajan, A., Sharma, K. G., Venkatachalam, K., and Abbas, S. M. (2002). "Constitutive modeling of rockfill materials from Tehri Dam, Uttaranchal." *Proc., Indian Geotechnical Conf.*, Indian Geotechnical Society, New Delhi, India, 592–595.
- Varadarajan, A., Sharma, K. G., Venkatachalam, K., and Gupta, A. K. (1997). "Constitutive modeling of a rockfill material using HISS model." *Proc., Indian Geotechnical Conf.*, Indian Geotechnical Society, New Delhi, India, 153–156.
- Varadarajan, A., Sharma, K. G., Venkatachalam, K., and Gupta, A. K. (1999). "Constitutive modelling of a rockfill materials." *Proc., 4th Int. Conf. on Constitutive Laws for Engineering Materials*, Rensselaer Polytechnic Institute, Troy, NY.
- Varadarajan, A., Sharma, K. G., Venkatachalam, K., and Gupta, A. K. (2003). "Testing and modeling two rockfill materials." *J. Geotech. Geoenviron. Eng.*, 10.1061/(ASCE)1090-0241(2003)129:3(206), 206–218.
- Vasistha, Y., Gupta, A. K., and Kanwar, V. (2012). "Prediction of shear strength parameters of two rockfill materials." *Electron. J. Geotech. Eng.*, 17(W), 3221–3232.
- Vasistha, Y., Gupta, A. K., and Kanwar, V. (2013). "Medium triaxial testing of some rockfill materials." *Electron. J. Geotech. Eng.*, 18(E), 923–964.
- Xiao, Y., Liu, H., Chen, Y., and Jiang, J. (2014a). "Bounding surface model for rockfill materials dependent on density and pressure under triaxial stress conditions." *J. Eng. Mech.*, 10.1061/(ASCE)EM.1943-7889.0000702, 04014002.
- Xiao, Y., Liu, H., Chen, Y., Jiang, J., and Zhang, W. (2014b). "Testing and modeling of the state-dependent behaviors of rockfill material." *Comput. Geotech.*, 61(Sep), 153–165.
- Xiao, Y., Liu, H., Chen, Y., and Zhang, W. (2014c). "Particle size effects in granular soils under true triaxial conditions." *Géotechnique*, in press.
- Xiao, Y., Liu, H. L., Zhu, J. G., and Shi, W. C. (2011a). "Dilatancy equation of rockfill material under the true triaxial stress condition." *Sci. China Tech. Sci.*, 54(S1), 175–184.
- Xiao, Y., Liu, H. L., Zhu, J. G., and Shi, W. C. (2012). "Modeling and behaviours of rockfill materials in three-dimensional stress space." *Sci. China Tech. Sci.*, 55(10), 2877–2892.
- Xiao, Y., Liu, H. L., Zhu, J. G., Shi, W. C., and Liu, M. C. (2011b). "A 3D bounding surface model for rockfill materials." *Sci. China Tech. Sci.*, 54(11), 2904–2915.
- Xu, M., Song, E., and Chen, J. (2012). "A large triaxial investigation of the stress-path-dependent behavior of compacted rockfill." *Acta Geotech.*, 7(3), 167–175.
- Yang, J., and Li, X. S. (2004). "State-dependent strength of sands from the perspective of unified modeling." *J. Geotech. Geoenviron. Eng.*, 10.1061/(ASCE)1090-0241(2004)130:2(186), 186–198.
- Zhang, B.-Y., Jie, Y.-X., and Kong, D.-Z. (2013). "Particle size distribution and relative breakage for a cement ellipsoid aggregate." *Comput. Geotech.*, 53(Sep), 31–39.
- Zhao, H. F., Zhang, L. M., and Chang, D. S. (2013). "Behavior of coarse widely graded soils under low confining pressures." *J. Geotech. Geoenviron. Eng.*, 10.1061/(ASCE)GT.1943-5606.0000755, 35–48.
- Zhou, W., Ma, G., Chang, X., and Zhou, C. (2013). "Influence of particle shape on behavior of rockfill using a three-dimensional deformable DEM." *J. Eng. Mech.*, 10.1061/(ASCE)EM.1943-7889.0000604, 1868–1873.